THE AMERICAN SOCIETY OF MECHANICAL ENGINEERS
345 E. 47 St., New York, N.Y. 10017

89-GT-69

An Experimental Study of Turbine Vane Heat Transfer with Leading Edge and Downstream Film Cooling

V. NIRMALAN and L. D. HYLTON

Allison Gas Turbine Division
General Motors Corporation
Indianapolis, Indiana

ABSTRACT

This paper presents the effects of downstream film cooling, with and without leading edge showerhead film cooling, on turbine vane external heat transfer. Steady state experimental measurements were made in a three-vane, linear, two-dimensional cascade. The principal independent parameters -- Mach number, Reynolds number, turbulence, wall-to-gas temperature ratio, coolant-to-gas temperature ratio, and coolant-to-gas pressure ratio -- were maintained over ranges consistent with actual engine conditions. The test matrix was structured to provide an assessment of the independent influence of parameters of interest, namely, exit Mach number, exit Reynolds number, coolant-to-gas temperature ratio, and coolant-to-gas pressure ratio.

The vane external heat transfer data obtained in this program indicate that considerable cooling benefits can be achieved by utilizing downstream film cooling. The downstream film cooling process was shown to be a complex interaction of two competing mechanisms. The thermal dilution effect, associated with the injection of relatively cold fluid, results in a decrease in the heat transfer to the airfoil. Conversely, the turbulence augmentation, produced by the injection process, results in increased heat transfer to the airfoil. The data presented in this paper illustrate the interaction of these variables and should provide the airfoil designer and computational analyst the information required to improve heat transfer design capabilities for film cooled turbine airfoils.

NOMENCLATURE

c_p	specific heat at constant pressure
Cr	correction factor for thermal entrance region effects
dT/dn	surface normal temperature gradient
h	heat transfer coefficient
Ma_2	downstream or vane row exit Mach number
P	plenum pressure
Re_2	downstream or vane row exit Reynolds number
S	percent surface distance
SNR	Stanton number reduction
St	Stanton number
T	temperature
u	freestream velocity
ρ	freestream density

subscripts

c	coolant plenum conditions
ds	downstream
FC	film cooled conditions
g	cascade inlet conditions
le	leading edge
NFC	non-film cooled conditions
o	reference
ps	pressure side
ss	suction side
s	surface static conditions
w	wall

INTRODUCTION

One of the classical ways to improve the thermal efficiency of a gas turbine engine is to increase the turbine inlet temperature. Today's advanced gas turbine engines operate at temperatures much greater than allowable metal temperatures of turbine airfoils, which in turn necessitates the cooling of airfoils. In addition, uniform airfoil cooling is also required to avoid thermal stresses. Some of the common methods of providing thermal protection to the airfoil are internal convective cooling and impingement cooling, external film cooling, and trailing edge ejection. A typical cooled airfoil incorporating all the above mentioned cooling techniques is shown in Figure 1. The degree of internal cooling must be limited because of the thermal stresses resulting from large thermal gradients in the metal wall. However, film cooling has the advantage that it provides thermal protection to the metal wall by the injection of cooler air over the external surface. To achieve uniform film cooling, it is necessary to inject coolant air at the leading edge and at multiple locations on the suction and pressure surfaces. Leading edge film cooling is generally accomplished by using a "showerhead" type of geometry of film cooling holes. Downstream pressure and suction surface film cooling are usually achieved by single or multiple rows of injection holes at comparable locations to the airfoil shown in Figure 1.

The thermal design of a typical film cooled blade, similar to the one shown in Figure 1, represents one of the more difficult engineering tasks. Aerodynamic and thermal procedures currently available to turbine designers have deficiencies that do not permit a priori designs that achieve design goals without expensive development iterations. Improvements in predictive capability of the cooling requirements have significant payoffs in terms of enhanced turbine life, development cost, and turbine

Presented at the Gas Turbine and Aeroengine Congress and Exposition—June 4-8, 1989—Toronto, Ontario, Canada
This paper has been accepted for publication in the Transactions of the ASME
Discussion of it will be accepted at ASME Headquarters until September 30, 1989

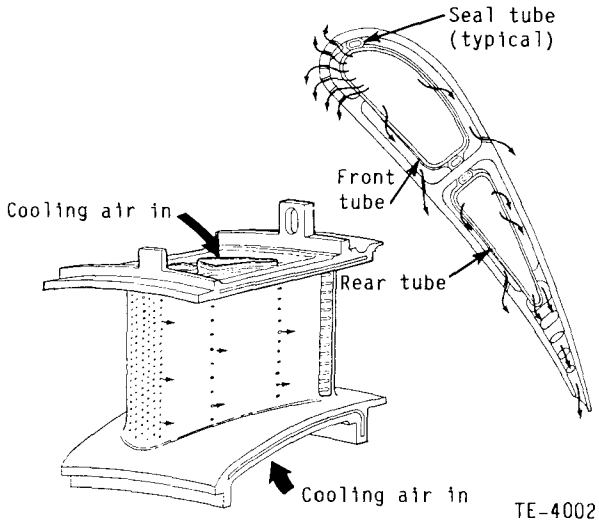

Figure 1. Typical cooled airfoil.

engine performance. One of the first steps in the development of a prediction tool is the availability of a relevant data base. The experimental measurements reported in this paper present external heat transfer data with downstream film cooling with and without leading edge showerhead film cooling. The data were obtained at conditions which fully simulate engine conditions of a first stage vane of an advanced turbine.

A review article on turbine blade cooling by Moffat (1986) indicates that the majority of data on film cooling in the literature has been obtained on flat plates and cylinders which were intended to simulate engine geometry. Recently, several film cooling studies on turbine airfoils have been conducted. Camci and Arts (1985a, 1985b) studied the effects of leading edge and suction side film cooling in a six airfoil cascade using the short duration measurement technique. Camci (1988) measured the heat flux near the film cooling hole on the suction side of a turbine blade previously investigated by Camci and Arts (1985b). Horton et al. (1985), also using the short duration measurement technique, measured heat transfer to turbine blades with suction and pressure side film cooling. Goldstein and Chen (1985) considered the effects of film cooling of a turbine blade near the end wall in a low speed wind tunnel using the mass/heat transfer analogy. Turner et al. (1985) conducted heat transfer measurements on a leading edge film cooled airfoil geometry using a three vane cascade at simulated engine conditions. A five-row simulated common plenum showerhead geometry was tested to determine the differences between film cooled and non-film cooled heat transfer coefficient distributions. This investigation is one of very few in the open literature that have been conducted at fully simulated engine conditions represented by the aerothermodynamic parameters such as Mach number, Reynolds number, wall-to-gas temperature ratio (T_w/T_g), coolant-to-gas temperature ratio (T_c/T_g), and turbulence intensity.

The objective of the investigation presented in this paper was to generate an engine representative data base of downstream film cooling with and without leading edge film cooling, thus extending the two earlier leading edge film cooling (Turner et al., 1985) and non-film cooled (Nealy et al., 1984) vane heat transfer studies conducted at Allison Gas Turbine Division. The aerodynamic configuration of the vane profile used in this study is the same as the one used in the leading film cooled experiments reported by Turner et al. (1985) and the same as one of the two airfoils used in the non-film cooled experiments reported by Nealy et al. (1984). The leading edge showerhead five row film cooling hole geometry in the present study is identical to the hole geometry of the earlier study (Turner et al., 1985). The airfoil in the current study had film cooling arrays added on the suction and pressure side, each consisting of two rows of holes. The three film cooling arrays were fed by separate plenums. The experiments were conducted in a moderate-temperature, three-vane, linear, two-dimensional cascade. Heat transfer data were acquired downstream of the pressure and suction surface film cooling arrays under steady state conditions. The principal independent parameters -- Mach number, Reynolds number, turbulence intensity, coolant-to-gas temperature ratio, and coolant-to-gas pressure ratio -- were maintained over ranges consistent with actual engine conditions, and the test matrix was structured to provide an assessment of the independent influence of parameters of interest, namely, exit Mach number, true chord exit Reynolds number, coolant-to-gas absolute temperature ratio, and coolant-to-gas pressure ratio.

In the following sections, descriptions of the hardware, instrumentation, and data reduction technique are given and the experimental results for surface pressure and heat transfer distributions are presented and discussed. Because of the large amount of data obtained in this investigation, only a summary of the data can be presented in this paper. More complete details are available in the report by Hylton et al. (1988).

EXPERIMENTAL APPARATUS AND PROCEDURES

Facility Description

This experimental investigation was performed in the Allison Gas Turbine (AGT) Aerothermodynamic Cascade Facility (ACF). The purpose of this facility is to conduct experimental research in high-temperature turbine component models that embody advanced cooling techniques, aerodynamics, or materials. The experimental approach employs a 2-D cascade technique, with full dynamic similarity in free-stream Mach number and boundary layer Reynolds number effects, and provides an experimental method to separate the effects on local heat transfer.

The facility consists of a burner, a convergent section, a free-stream section with instrumentation and optical access, a test section with instrumentation, a quench zone with back pressure regulation and an exhaust system. The facility is shown schematically in Figure 2.

The Mach number and Reynolds number modeling considerations necessitate a burner with a large temperature, flow, and pressure range. This burner capability, coupled with back pressure regulating valve, allows experimental separation of free-stream Mach number and boundary layer Reynolds number effects to accurately simulate a wide range of engine designs and operating conditions.

A constant cross section is provided downstream of the burner to establish uniform inlet velocity, temperature, and turbulence profiles. This section is provided with temperature-controlled cooled walls and isolates the test section from radiant heat transfer from the primary combustion zone. The walls of the test section are cooled with steam to keep them at, or close to, the vane surface temperature to eliminate radiation errors in the data.

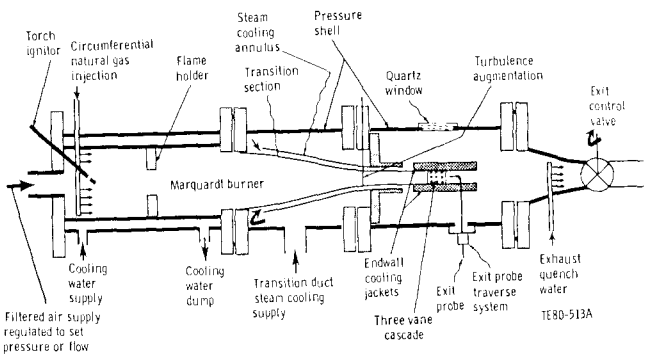

Figure 2. Schematic of Aerothermodynamic Cascade Facility.

The flow path upstream of the cascade in the ACF takes the burner discharge from a 0.315 m diameter through a 0.508 m long transition section to a 0.076 m x 0.279 m rectangular section. The rectangular section upstream of the cascade is 0.368 m long and contains inlet instrumentation. Details of the inlet and exit instrumentation are reported by Hylton et al. (1988).

Facility operations and data acquisition are handled by a dedicated, state-of-the-art computer-controlled data acquisition system. A multi-task, facility-oriented software system that contains general subprograms to do all routine control measurement tasks exists. The system is flexible and provides for real-time facility monitoring and diagnosis of instrumentation or control problems. Software routines developed to meet specific data acquisition requirements of individual experiments are incorporated into the main system as interchangeable program segments.

Cascade Description

The three-vane cascade employed in this test was the C3X cascade previously used in the earlier experimental studies reported by Turner et al. (1985) and Nealy et al. (1984). The center test vane was replaced with a new C3X vane which had suction side, leading edge, and pressure side film cooling arrays. The test vane, which has a nominal chord of 14.5 cm and span of 7.6 cm, was initially fabricated as a single piece. After all the film cooling holes and plenums and the ten radial cooling holes were machined, the vane was cut into a nose and a tail piece to form a thermal barrier between the film cooled nose piece and the rest of the vane.

The test vane was internally cooled by an array of 10 radial cooling holes, the locations of which are shown in Figure 3. Each hole in the center test vane was supplied from a separate, metered line.

The film cooling geometry for the test vane consists of film cooling arrays on the leading edge, the suction surface, and the pressure surface. The leading edge film cooling geometry employed a showerhead array of five equally spaced rows of holes with the center row located at the predicted aerodynamic stagnation point. The hole array is staggered with the holes in the second row located midway (radially) between the holes in the first and the third rows. The holes are angled at 45 degrees to the surface in the radial (spanwise) direction (slant angle). They are normal to the surface in the chordwise direction (skew angle). Coordinates of the film cooling hole rows are also listed in Figure 3. Geometry information for all film cooling arrays is detailed in Table I.

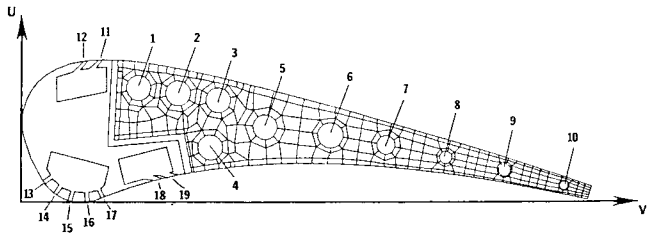

Radial cooling holes					Film cooling holes		
Hole No.	U, mm	V, mm	Diameter, mm	Cr	Hole No.	U, mm	V, mm
1	26.70	29.92	6.30	1.118	11	35.92	20.24
2	27.33	39.98	6.30	1.118	12	35.56	16.31
3	25.55	49.91	6.30	1.118	13	4.98	5.41
4	13.64	47.88	6.30	1.118	14	2.11	8.28
5	18.69	61.82	6.30	1.118	15	0.41	11.96
6	16.66	77.47	6.30	1.118	16	0.05	16.00
7	14.12	92.35	4.70	1.090	17	1.09	19.94
8	10.87	107.59	3.10	1.056	18	5.59	35.05
9	7.37	122.53	3.10	1.056	19	6.43	38.91
10	3.45	137.57	1.98	1.025			

Figure 3. Film cooled C3X vane showing internal geometry and finite element grid

Table I.
Film cooling hole geometry

Leading edge geometric parameters	Values
Rows of holes	5
Hole diameter, mm	0.99
Hole length, mm	3.35
Hole pitch-to-diameter ratio	4.0
Hole spacing-to-diameter	7.5
Hole slant angle, deg	45
Hole skew angle, deg	90

Downstream geometric parameters	Values
Rows of holes (each surface)	2
Hole diameter, mm	0.99
Hole length, mm	3.35
Hole pitch-to-diameter ratio	4.0
Hole spacing-to-diameter	3.0
Hole slant angle, deg	90
Hole skew angle, deg	
Pressure surface	20
Suction surface	35

Previous leading edge film cooling data of Turner et al. (1985) indicated that the downstream film cooling arrays should be located at 25.2% of the surface distance (as measured from the geometric stagnation point, which is defined as the tangency point on the airfoils of the inlet plane to the cascade) on the suction side and 22.5% of the surface distance on the pressure side. This is just upstream of the suction and pressure surface pressure recovery region in the non-film cooled case and thus appear to provide maximum film cooling effectiveness. Two cooling hole rows were centered on each surface at these points. The downstream film cooling hole arrays are also staggered with the holes in the second row located midway (radially) between the holes of the first row. The length-to-diameter ratio of the holes were kept the same as the showerhead hole length-to-diameter ratio. The suction surface holes were inclined at 35 degrees to the surface in the chordwise direction while the pressure surface holes were at 20 degrees in the chordwise direction. Holes in both downstream arrays were normal to the surface in the spanwise direction.

Three independent supply plenums were designed to feed the three film cooling arrays as shown in Figure 3. This system was designed to provide the capability of individually controlling the blowing parameters of each array. The relatively large plenum resulted in a nearly uniform coolant flow distribution in the spanwise direction. The film coolant supply was piped through an electric heating system that provided the capability to vary the coolant supply temperature.

The heat transfer measuring technique used for this test does not make heat transfer measurements in the actual film cooled nose piece. Consequently, the film cooled area was thermally isolated from the rest of the airfoil. As mentioned before, the thermal barrier was achieved by cutting the test vane into two segments, with the airfoil profile maintained in its original contour by two retaining bars pinned to the airfoil ends. Prior to testing, a thin, 0.254 mm shim was welded across the thermal barrier gap on both the pressure and suction surfaces. This provided a smooth continuous surface on the airfoil. Also, the gap was sealed at the two ends of the airfoil, thereby creating a sealed air gap between the film cooled region and the rest of the airfoil. The sealed air gap provided the thermal barrier.

Instrumentation

Figure 4 shows the distribution of the thermocouples and pressure taps for the C3X airfoil. The airfoil surface was instrumented with 123 0.51 mm diameter sheathed Chromel-Alumel (CA) thermocouples, while the thermal barrier region was instrumented with 18 1.02 mm CA thermocouples. The thermocouple junctions were located in the fully 2-D

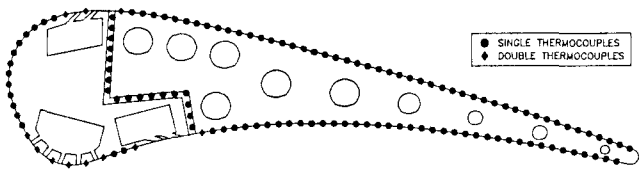

(a) Thermocouple locations

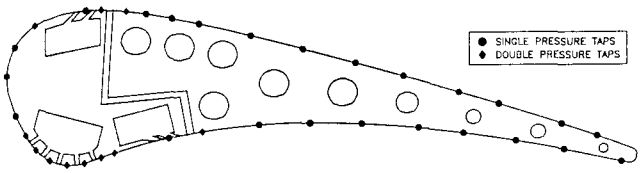

(b) Pressure tap locations

Figure 4. Instrumentation location for the C3X airfoil.

region of the airfoil in a plane 2.54 mm off midspan. While the thermocouples were located directly downstream of film cooling holes, the fact that this was an engine-like environment and not an adiabatic test, surface conduction effects resulted in uniform spanwise temperature, gradients similar to what occurs in an engine. Thermocouples were brought off the vane in 0.58 mm deep radial grooves covered with cement, and blended by hand to provide a smooth surface. The vane was fabricated of ASTM type 310 stainless steel, which has a relatively low thermal conductivity, thereby minimizing the error introduced by the grooves.

The test vane surface was also instrumented with surface static pressure taps in addition to the heat transfer instrumentation. Forty-six taps were located around the airfoil outer surface in a plane 5.08 mm from midspan away from the thermocouple instrumentation. The pressure taps were located so that the taps would be downstream of a film cooling hole. The spacing was varied to provide a higher density of instrumentation in high pressure gradient regions. Figure 4(b) illustrates the relative locations of the surface pressure taps on the C3X airfoil. Stainless steel tubing, 0.51 mm diameter, was laid in a radial surface groove, and the end of the tubing was bent 90 degree to achieve surface orientation.

In addition to the thermocouples on the instrumentation plane, twelve extra thermocouples were placed on the suction and pressure surfaces, 19.05 mm on either side of the instrumentation plane at three axial locations. These and the instrumentation plane temperatures at the same axial locations provided a check on the validity of the two dimensionality of the heat transfer solution.

Each of the tubes supplying the radial cooling holes of the test vane was instrumented with two static pressure taps and two thermocouples at both the vane inlet and exit. The static pressure taps were located upstream of the thermocouples in all cases. The flow to each cooling tube was measured using a calibrated orifice meter.

Each film cooling plenum was instrumented with thermocouples and pressure taps at various locations to provide the coolant supply temperature and pressure. The flow rate to each plenum was measured using a calibrated orifice meter.

Data Reduction Procedure

The method used to obtain heat transfer measurements is based on the work of Turner (1971), who employed a 2-D plane of a test piece as a fluxmeter. The technique is implemented by measuring the internal and external boundary conditions of the test piece at thermal equilibrium and solving the steady-state heat conduction equation for the internal temperature field of the test piece. The heat transfer coefficient distribution can be directly obtained from the normal temperature gradient at the surface.

For the present study, the heat transfer measurement technique used a finite element solution of 2-D Laplacian heat conduction equation as illustrated in Figure 5. The finite element grid structure actually used for the solution was shown in Figure 3. The external boundary conditions were measured using the thermocouples installed in grooves on the exterior surface of the test vane and in the thermal barrier on the tail piece of test vane. Average heat transfer coefficients and coolant temperatures for each of the 10 radial cooling holes provided the internal boundary conditions for the finite element solution. The heat transfer coefficient for each cooling hole was calculated, using standard correlations, from the hole diameter, measured coolant flow rate, and coolant temperature with a correction applied for thermal entry region effects.

The accuracy of the external heat transfer coefficient measurement is primarily dependent on the accuracy of the external vane surface and free-stream gas temperature measurements, the geometry description for the finite element program, the calculation of the heat transfer coefficients for the radial cooling holes, and the knowledge of the thermal conductivity of the vane material. Using the uncertainties of the individual measurements, a calculation of the overall uncertainty in the external heat transfer coefficient was made using the methods of Kline and McClintock (1953). Due to variations in the airfoil thickness along the chord, it was necessary to calculate the uncertainty at several points. The maximum uncertainty, based on minimum wall thickness (distance from cooling hole to exterior surface), was calculated at various regions on the airfoil. The values ranged from ± 7.1% to ± 22.5%. The uncertainties increase significantly beyond midchord due to a decrease in airfoil thickness. The uncertainties presented are intended to provide the analyst with an indication of the uncertainty in absolute levels in using the data for verification purposes. In comparing data runs for a given cascade (i.e., looking for Reynolds number trends, etc), the uncertainty in the comparisons is considerably less than the values just described. This difference is due to the fact that several of the variables contributing to the uncertainty do not change from run to run. Reproducibility of heat transfer coefficients for a given cascade condition is on the order of ± 2%.

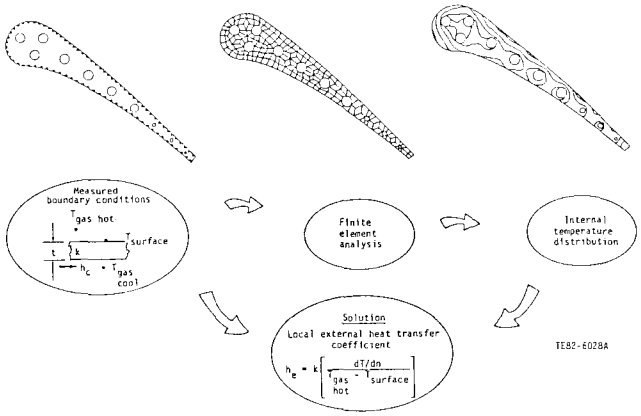

Figure 5. Heat Transfer Data Reduction Technique

RESULTS

Range of Experimental Conditions

The experimental results presented in this study were obtained at different test conditions with the variable parameters being exit Reynolds number, exit Mach number, coolant-to-gas absolute temperature ratio and coolant-to-gas total pressure ratio. The nominal run conditions where heat transfer data were obtained are shown in a graphical form in Figure 6. Each nominal test condition is represented by a five-digit alphanumeric code. Each alphanumeric digit of the code number corresponds to one of the control variables of the experiment as also described in Figure 6. Exit Reynolds numbers referred to in the figure are based on airfoil true chord (not axial chord), and exit Mach numbers are based on measured inlet total pressure and mid-passage to mid-passage average measured exit plane static pressure. All tests were conducted at a nominal gas stream temperature of 700 K, and a burner generated turbulence intensity level of 6.5%, based on LDA measurements taken previously at the cascade inlet plane as reported in Nealy et al. (1984).

Airfoil Static Pressure Distributions

Prior to obtaining film cooled data, baseline data (i.e., without film cooling) were obtained at the seven baseline conditions as shown in Figure 6. Starting first with the exit Mach number effects, typical baseline measured surface static pressure distributions corresponding to the four cascade expansion ratios tested are shown in Figure 7. The percent surface distance in Figure 7 and all figures that follow is measured from the geometric stagnation point. In this figure and in other similar figures, the vertical dashed lines mark the locations of the film cooling hole rows and the vertical solid lines mark the locations of the thermal barrier on the pressure and suction surfaces. As observed by Turner et al. (1985) and Nealy et al. (1984), at the transonic exit Mach numbers of 0.9 and 1.05,

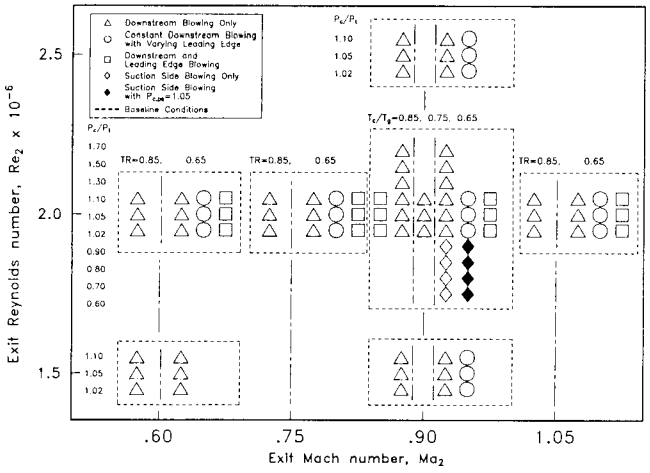

Code No.	Control variable by position					
	Position 1--Ma_2	Position 2--$Re_2 \times 10^{-6}$	Position 3--T_c/T_g	Position 4--$P_{c,le}/P_t$	Position 5--$P_{c,ds}/P_t$ ss	ps
0			No coolant flow	1.00	1.00	1.00
1			Min			
2	0.60		Med			
3	0.75	1.5	Max	1.02	1.02	1.02
4	0.90	2.0		1.05	1.05	1.05
5	1.05	2.5		1.10	1.10	1.10
6					1.30	1.30
7					1.50	1.50
8					1.70	1.70
A					0.60	1.00
B					0.70	1.00
C					0.80	1.00
D					0.90	1.00
E					0.60	1.05
F					0.70	1.05
G					0.80	1.05
H					0.90	1.05

Figure 6. Test matrix and control code description.

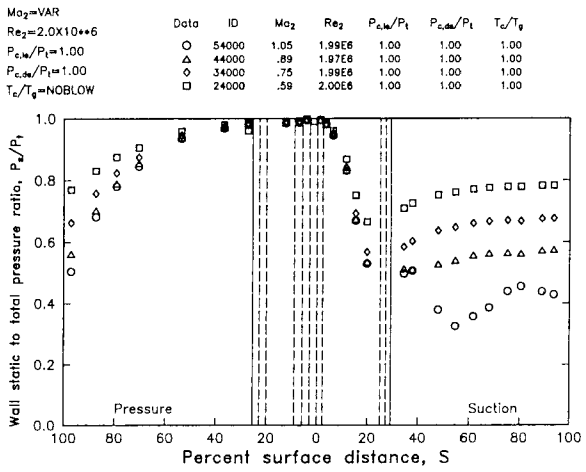

Figure 7. The effects of exit Mach number variation on baseline static pressure distribution.

the primary effect of exit Mach number variation is to alter the suction surface pressure distribution downstream of the throat. However, at the lower Mach numbers of 0.6 and 0.75, larger differences in surface static pressure due to Mach number variations are seen on both surfaces; at surface distances of 60% and greater on the pressure surface and at 15% and greater on the suction surface.

The effect of downstream blowing on the vane surface static pressure distribution is shown in Figure 8, where the base flow conditions are at an exit Mach number of 0.9 and an exit Reynolds number of 2.0×10^6. Figure 8 indicates that increasing the downstream blowing strength from a coolant-to-freestream pressure ratio of 1.00 (no blowing) to 1.63 has no measurable effect on the vane surface static pressure distribution.

Heat Transfer Results

The measured baseline heat transfer for different Mach numbers is shown in Figure 9. On the suction surface, the level of heat transfer coefficient decreases with increasing exit Mach number due to different static pressure distribution. On the pressure surface, much less variation in heat transfer due to variation in Mach number is noticed, again caused by lesser variation in the static pressure distribution. The effect of exit Reynolds number variation on the baseline heat transfer coefficient distribution is shown in Figure 10. As expected, the overall heat transfer levels systematically increase as the exit Reynolds number increases.

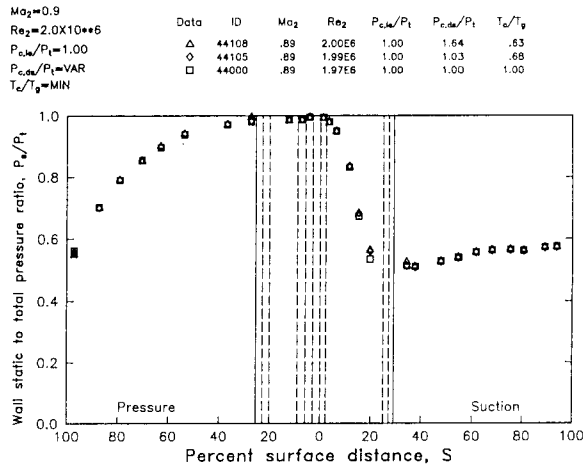

Figure 8. Effects of downstream blowing on surface static pressure distribution.

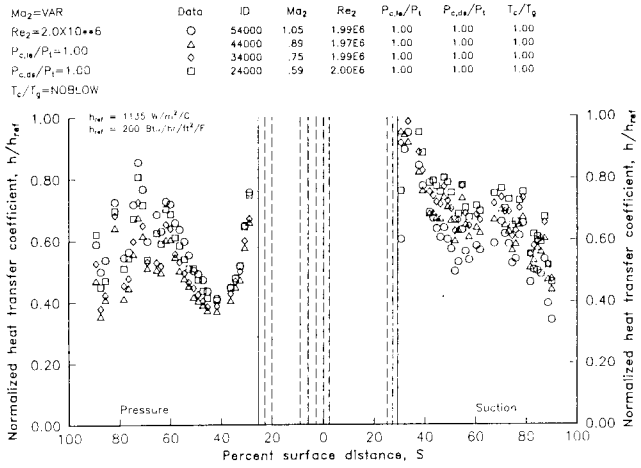

Figure 9. Effects of exit Mach number variation on baseline heat transfer coefficient distribution.

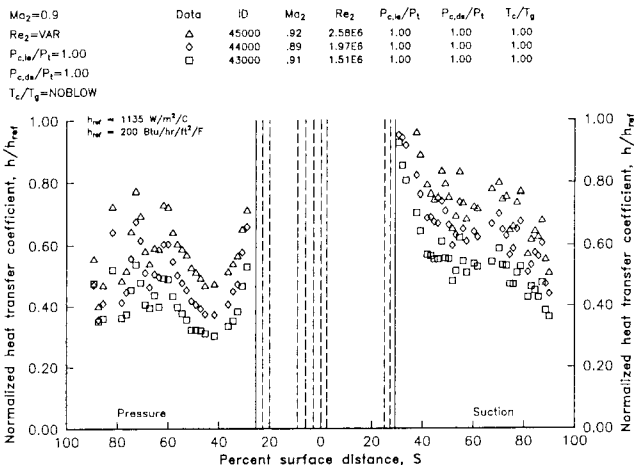

Figure 10. Effects of exit Reynolds number variation on baseline heat transfer coefficient distribution.

The present baseline heat transfer data matches reasonably well with the previously obtained data of Turner et al. (1985) and Nealy et al. (1984) at surface percentage distances greater than 50% on both suction and pressure surfaces. However, at surface distances less than 50%, the differences in film cooling geometry between the vane of the present study and the previous studies causes differences in absolute heat transfer data. In the present study, during baseline runs, there is a developing thermal boundary layer which begins at the thermal barrier. This occurs on both surfaces at about 20-25% surface distances and results in differences in absolute heat transfer levels at surface distances less than 50%. In the case of a vane which is uniformly cooled throughout, the hydrodynamic and the thermal boundary layer would originate simultaneously at the leading edge. However in the present study, under non-film cooled conditions, the nose piece of the vane is not cooled (radially or otherwise). This results in a step change in vane surface temperature across the thermal barrier on both surfaces as shown in Figure 11, which gives the vane surface-to-gas absolute temperature ratio (T_w/T_g) distribution at the baseline condition corresponding to an exit Mach number (Ma_2) of 0.9 and exit Reynolds number (Re_2) of $2.0x10^6$. This indicates that the origin of the thermal boundary layer is at the thermal barrier, while the hydrodynamic boundary layer still originates at the leading edge. In Figures 9 and 10, the decreasing slope of the heat transfer coefficient downstream of the thermal barrier on both surfaces is a result of the developing thermal boundary layer.

Also, in Figure 11, a spatial variation in vane surface temperatures is seen near the trailing edge on both surfaces. These variations are due to coolant air flowing through the internal cooling holes. These variations in surface temperature result in the heat transfer coefficient fluctuations seen earlier in Figures 9 and 10. Figure 12 repeats the measured heat transfer distribution for the baseline condition of Ma_2 = 0.9 and Re_2 = $2.0x10^6$, which again shows the fluctuations in heat transfer coefficient over the rear 50 percent of the airfoil. Also in Figure 12, results predicted (Hylton et al., 1987) for the same conditions using the Allison - STANCOOL code developed by Turner et al. (1985) are given. Here, the solid curve is the predicted results with a constant temperature boundary condition. The dashed curve is the prediction made using the actual measured surface temperature boundary condition given in Figure 11. Figure 12 shows significantly better agreement between the experimental data and the prediction using the measured surface temperature for the boundary condition. Considering the uncertainty in absolute value of the experimentally determined heat transfer coefficient, the agreement is quite good. This comparison illustrates the significance of the actual wall temperature boundary condition on the heat transfer predictions.

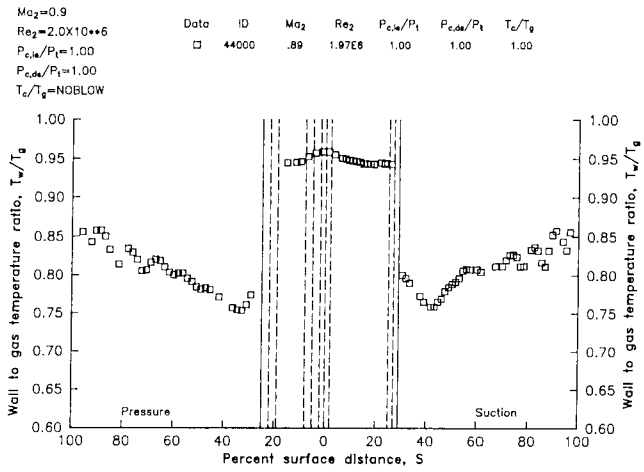

Figure 11. Surface-to-gas absolute temperature distribution at baseline flow condition of Ma_2 = 0.9 and Re_2 = $2.0x10^6$.

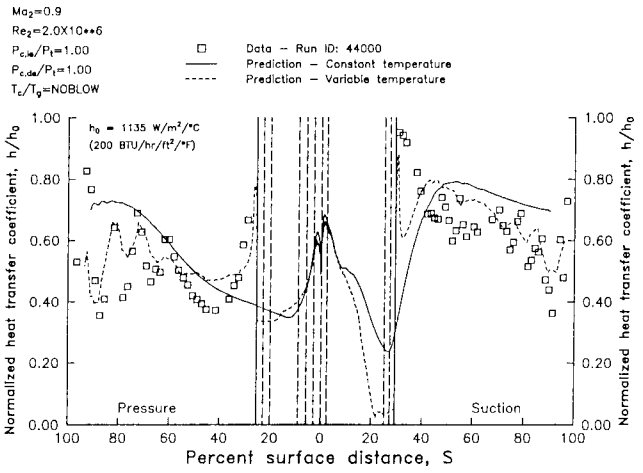

Figure 12. Surface local heat transfer distribution at baseline flow condition of Ma_2 = 0.9 and Re_2 = $2.0x10^6$.

The goal of presenting the film cooled heat transfer results is to isolate the differences between non-film cooled and film cooled (in this case, downstream film cooling with and without leading edge injection) heat transfer downstream of the suction and pressure side film cooling arrays. This goal is achieved, as done before by Turner et al. (1985), by calculating the ratio of the experimentally determined local Stanton number for cases where coolant is being ejected to the local Stanton number determined for the case where no coolant is added.

Rather than simply form the film cooled Stanton number to non-film cooled Stanton number ratio (St_{FC}/St_{NFC}), which would take on values about a "no difference" value of unity, an alternate parameter referred to as Stanton number reduction (SNR) is used. SNR is defined as

$$SNR = 1 - (St_{FC}/St_{NFC})$$

When SNR is greater or less than zero, it implies reduced or increased heat transfer levels, respectively. When SNR is equal to zero, it implies no difference in the heat transfer level. Forming SNR values along the entire test surface gives the actual SNR distribution for the airfoil. In addition, if the film cooled Stanton number to non-film cooled Stanton number ratio were determined using data obtained at equivalent exit Mach number and exit Reynolds number conditions, SNR would be approximately equal to the actual heat transfer coefficient reduction

$$SNR = 1 - (h_{FC}/h_{NFC})$$

because $(\rho c_p u)_{e,NFC}/(\rho c_p u)_{e,FC}$ would be near unity. SNR results shown here were formed by using the above equation. Basic heat transfer coefficient and wall temperature data are available in the final report of Hylton et al. (1988).

Figure 13 shows the effects of varying the blowing strength at two constant thermal dilution (T_c/T_g) levels with only the downstream film cooling arrays active. The base flow conditions are at an exit Mach number of 0.9 and an exit Reynolds number of 2.0×10^6. Figure 13(a) shows the effect of varying blowing strength (P_c/P_t) at the lowest coolant-to-gas temperature ratio (T_c/T_g = 0.65, MIN). [Film cooling flow rate, absolute pressure, etc. are available in the final report (Hylton et al., 1988). Coolant hole exit temperatures, if desired, can be calculated from heat pickup estimations using the information available in the final report.] A positive SNR is seen on both surfaces at all three blowing strengths indicating a comparatively large decrease in heat transfer due to downstream film cooling. A pronounced variation in SNR due to different blowing strengths is seen on the pressure surface. Also, on the pressure surface, as the blowing strength is increased, the effect of film cooling is felt further downstream. However, the higher turbulence level near the film cooling holes, resulting from increased blowing, tends to increase heat transfer (i.e, reduce SNR) in the near hole region. On the other hand, on the suction surface, there is no significant effect due to varying blowing strengths. This is due to the lower freestream pressure on the suction surface causing the film coolant flow on the suction surface to be choked over this range of pressure ratios. The choked conditions keep the blowing ratio almost invariant on the suction surface. Figure 13(b) shows similar behavior at a higher T_c/T_g ratio of 0.85 (MAX), though, as expected, with lower values of SNR due to the lower level of thermal dilution (warmer air being injected). Also, on the pressure surface at the lower thermal dilution level (high T_c/T_g), the effect of turbulence due to the higher blowing strengths increases heat transfer (i.e., decreases SNR values) just downstream of the film cooling holes to a larger extent than at higher thermal dilution level (i.e., low T_c/T_g). It should also be noted that for the higher blowing strengths, SNR increases over the last 60% of the airfoil; where as, for the lower blowing strengths, the SNR decreases. This is the result of the interaction of the thermal dilution and turbulence augmentation effects. On the SNR data presented above, just downstream of the suction side film cooling holes, SNR attain high values. These high SNR values are caused by the non-film cooled and the film cooled tests having different surface temperatures in the leading edge region. In a film cooled case, the surface temperature in the leading edge region, in contrast to the surface temperature shown in Figure 11, would be much lower and

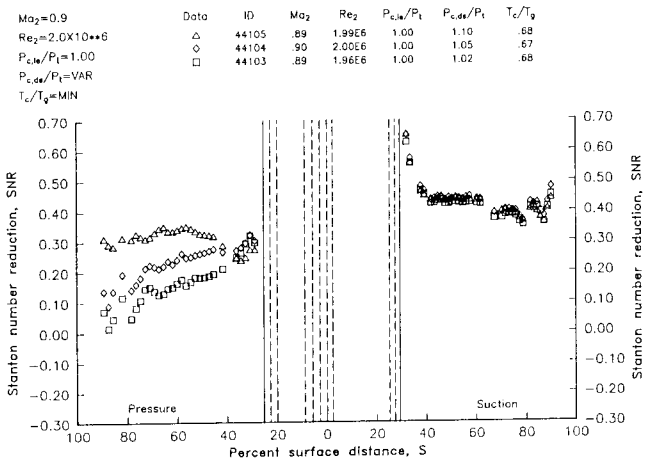

(a)T_c/T_g = MIN

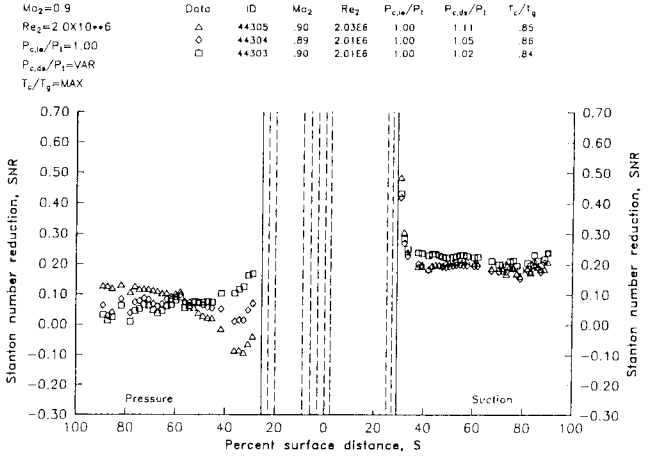

(b)T_c/T_g = MAX

Figure 13. Effects of downstream blowing on Stanton number reduction

nearly at the same levels as the rest of vane surface. Therefore when comparing film cooled data to non-filmed cooled data there are apparent high SNR values just downstream of the thermal barrier.

The same trends noticed above are further brought out by Figure 14, which shows data with downstream film cooling holes active for blowing strengths at levels up to 1.7 at MIN and MAX levels of thermal dilution. On the pressure surface, at both coolant-to-gas temperature ratios, the turbulence due to high blowing strengths decrease the SNR near the film cooling holes. At the lower coolant-to-gas temperature ratio, as shown in Figure 14(a), a positive value of SNR is seen, even at the highest blowing strength. However, in Figure 14(b), at the higher coolant-to-gas temperature ratio, almost all the data on the pressure surface at high blowing strengths (P_c/P_t > 1.3) show negative SNR values. (Note that in Figure 14(b), the SNR scales are offset.) On the other hand, there is hardly any effect of coolant pressure on the suction surface due to the fact that the film coolant flow is choked and no significant variation in blowing ratio occurred. Nevertheless, at the higher coolant-to-gas temperature ratio, on the suction surface, there is a slight decrease in SNR near the film cooling holes at the high blowing strengths. Although the

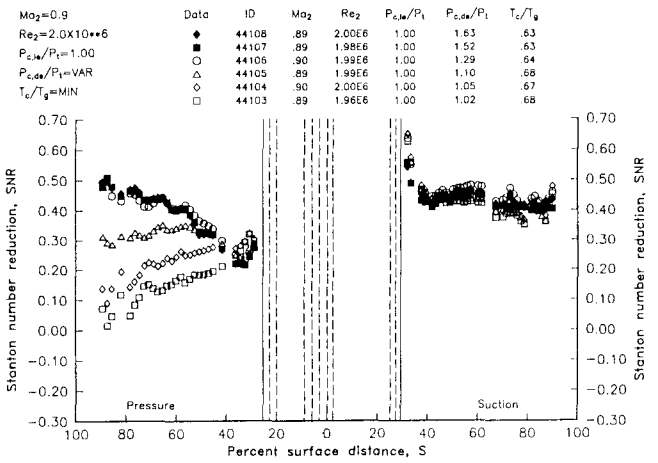

(a)T_c/T_g = MIN

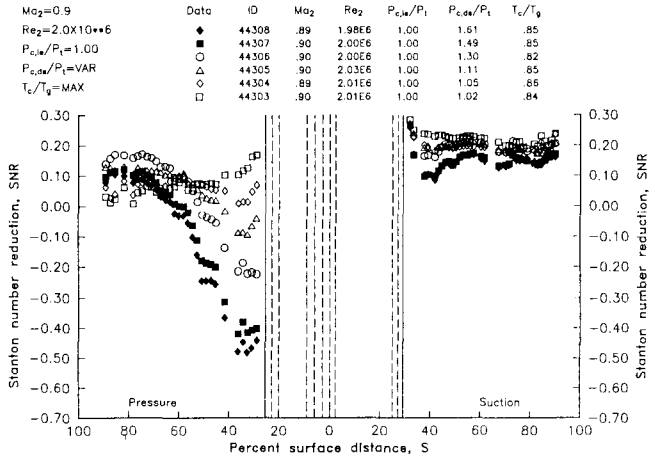

(b)T_c/T_g = MAX

Figure 14. Effects of high downstream blowing on Stanton number reduction.

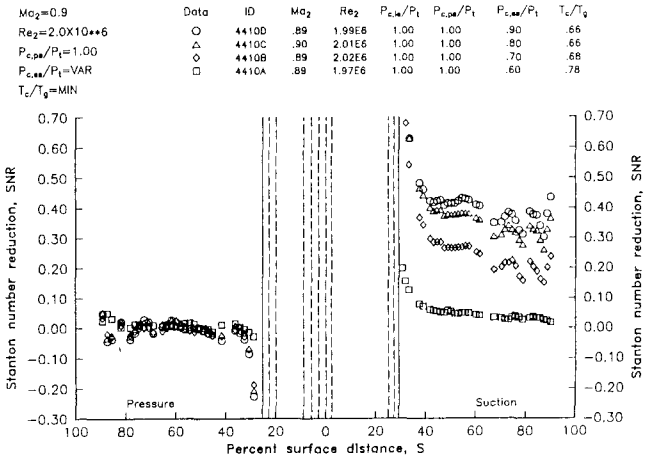

(a)$P_{c,ps}/P_t$ = 1.00

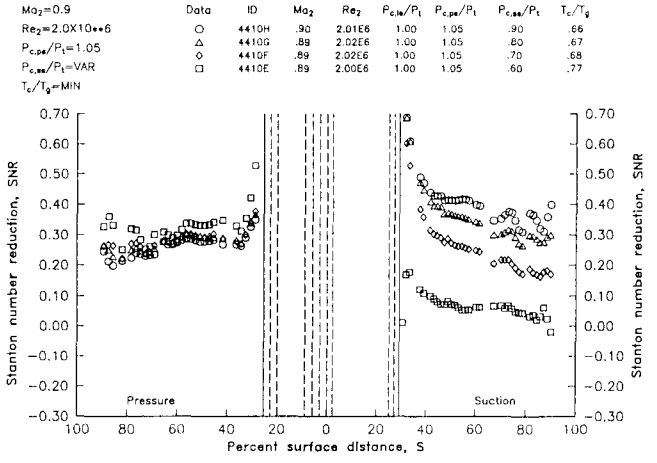

(b)$P_{c,ps}/P_t$ = 1.05

Figure 15. Effects on Stanton number reduction of variable suction side blowing at reduced pressure ratio.

flow is choked, increasing coolant supply pressure increases the coolant mass supply, causing an increase in turbulence level near the coolant holes, which in turn reduces SNR at very high blowing strengths. This also may be due to the damping of turbulence at increased velocity levels.

Figure 15 shows the effects of varying only the suction side blowing strength ($P_{c,ss}/P_t$) from 0.6 to 0.9, with the pressure side blowing strength ($P_{c,ps}/P_t$) kept constant at two levels of 1.00 (no blowing) and 1.05, respectively. These data are at flow conditions of Ma_2 = 0.9 and Re_2 = $2.0x10^6$ and the coolant-to-gas temperature ratio at MIN level. Figure 15 shows that the SNR on the suction side increases with increasing blowing strength until the coolant flow chokes. Also, these data indicate, as expected, that the performance of the two downstream film cooling arrays are independent of each other.

To illustrate the effects of thermal dilution, data shown earlier in Figure 13 were re-plotted with additional data as a function of T_c/T_g at two blowing strengths of 1.02 and 1.10 and are shown in Figure 16. On the suction surface, in both cases, there is a significant effect due to different coolant-to-gas temperature ratios. Conversely, on the pressure side, at the lower blowing strength, as shown in Figure 16(a), only a small effect is noticed. However, as seen in Figure 16(b), there is a larger effect on the pressure surface due to varying thermal dilution at the higher blowing strength of P_c/P_t = 1.10. Also in Figure 16(b), at higher coolant-to-gas temperature ratio, SNR is negative on the pressure surface at surface distances less than 50%. As mentioned before, this increase in heat transfer is due to the high blowing strength causing a higher level of turbulence augmentation which offsets the thermal dilution effects in the vicinity of the film cooling holes.

Figure 17 illustrates the effect of varying the exit Mach number from 0.6 to 1.05 while keeping other flow and film cooling conditions constant. In these instances, the downstream film cooling hole arrays are at blowing strengths, $P_{c,ds}/P_t$, of 1.10 and the coolant-to-gas temperature ratios, T_c/T_g, are at MIN (Figure 17(a)) and MAX (Figure 17(b)) levels. In these cases, each film cooling data point is compared with the baseline at that flow condition. In other words, these SNR data show the increase or decrease of the heat transfer over the particular baseline case. Figure 17 shows that there is no significant effect of SNR due to variations in Mach number on either the suction surface or pressure surfaces at the lower coolant-to-gas temperature ratio. However, on the pressure surface at the higher coolant-to-gas temperature ratio, Figure 17(b) shows that there is a Mach number effect. As pointed out earlier, at the higher coolant-to-gas temperature ratio, on the pressure surface, the favorable thermal dilution

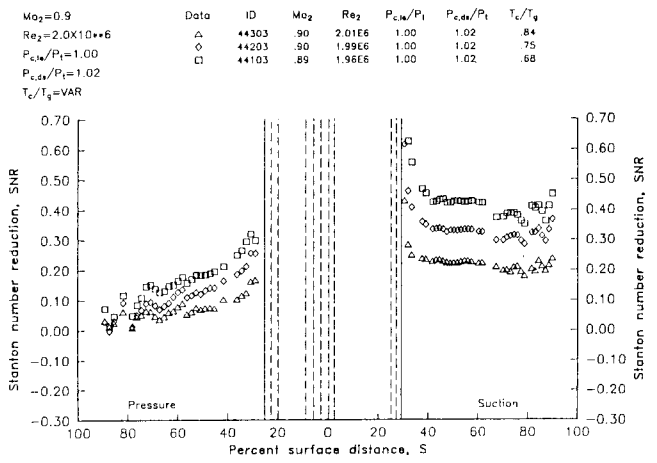

(a)P_c/P_t = 1.02

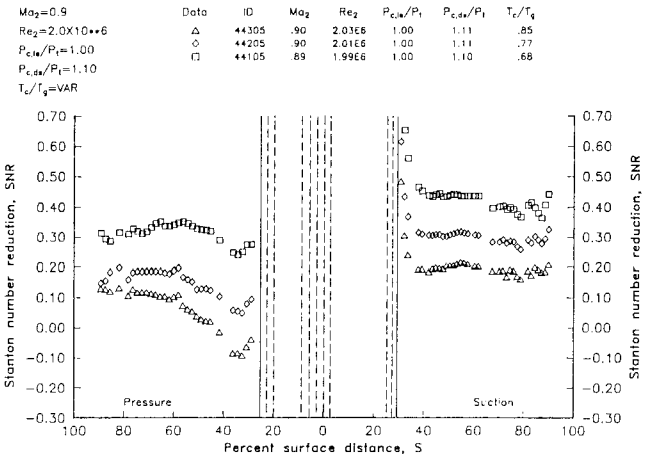

(b)P_c/P_t = 1.10

Figure 16. Effects on downstream film cooling thermal dilution on Stanton number reduction.

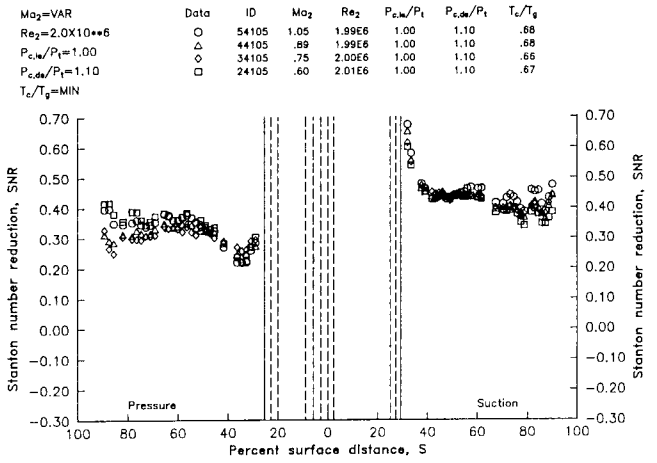

(a)T_c/T_g = MIN

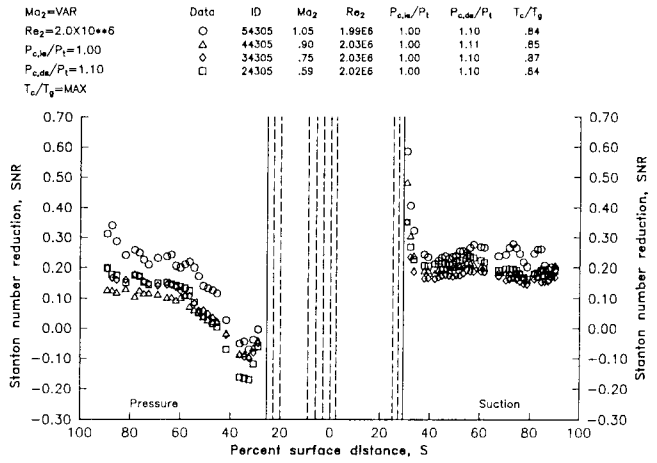

(b)T_c/T_g = MAX

Figure 17. Effects of exit Mach number on Stanton number reduction.

effects are offset by the adverse turbulence augmentation effects, thereby increasing heat transfer near the vicinity of the film cooling holes. For regions where this phenomenon occurs, the change in heat transfer due to film cooling seems to depend on the Mach number, suggesting that the turbulent augmentation effect may be Mach number dependent.

The effects of three different exit Reynolds numbers of $1.5x10^6$, $2.0x10^6$, and $2.5x10^6$ on downstream film cooling are shown in Figure 18. As in Figure 17, the SNR data show the change in heat transfer due to film cooling above the particular baseline. Figure 18(a) presents data at the MIN level of coolant-to-gas temperature ratio and coolant pressure ratio of 1.10. On both surfaces, SNR increases with increasing Reynolds number indicating that a more favorable effect of film cooling is attainable at a higher Reynolds number, though the trends are more pronounced on the pressure surface than on the suction surface. In Figure 18(b), where the coolant-to-gas temperature is at MAX level, the effect of Reynolds number variation is not as marked as in the case of the lower coolant-to-gas temperature ratio.

Figure 19 shows the effects of both the downstream and the leading edge film cooling arrays being active with the varying blowing strengths at the MIN and MAX levels of thermal dilution, respectively. The flow conditions are at an exit Mach number of 0.9 and exit Reynolds number of $2.0x10^6$. In comparison to Figure 13, the trends and levels of SNR are very similar to the case where only the downstream film cooling holes are active. However, comparing Figures 13 and 19, on the pressure surface just downstream of the film cooling holes, slightly higher values of SNR are seen due to the leading edge film cooling holes being active.

The SNR data for the case where downstream film cooling hole arrays are at a constant blowing strength of 1.10 while the leading edge film cooling blowing strength is varied from 1.00 (no leading edge blowing) to 1.10 are shown in Figure 20. These data are at the flow conditions corresponding to an exit Mach number of 0.6 and an exit Reynolds number of $2.0x10^6$. On the pressure surface, SNR is increased by low leading edge blowing values ($P_{c,le}/P_t$ = 1.02). However, at higher leading edge blowing values, SNR values drop off, to the extent that SNR is lower than without any leading edge blowing. This indicates that high leading edge blowing rates can actually increase heat transfer over the entire pressure surface of the airfoil due to increased turbulence levels. On the other hand, very little effect of leading edge blowing is seen on the suction surface.

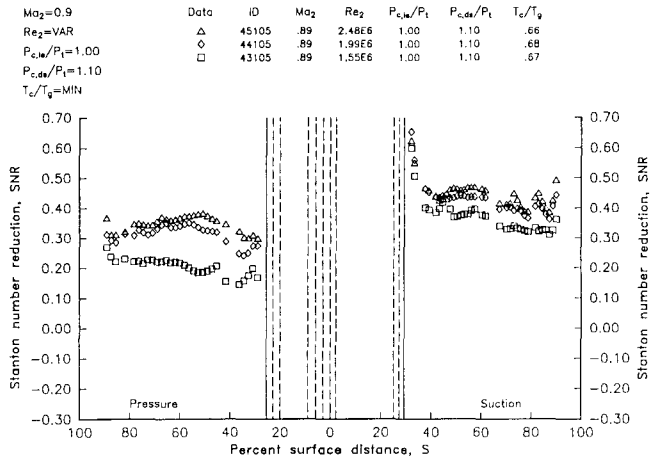

(a)T_c/T_g = MIN

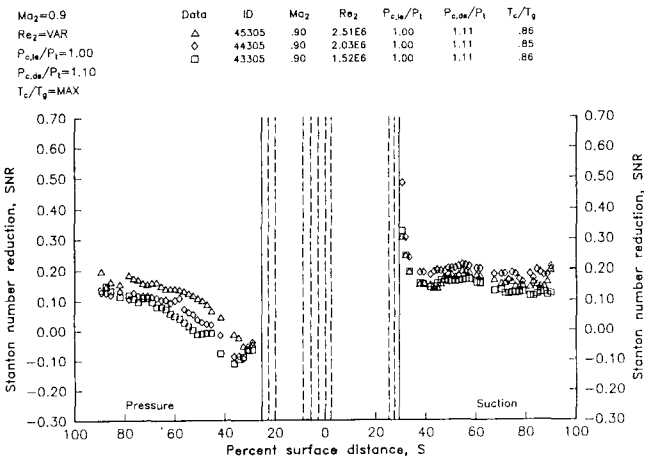

(b)T_c/T_g = MAX

Figure 18. Effects of exit Reynolds number on Stanton number reduction.

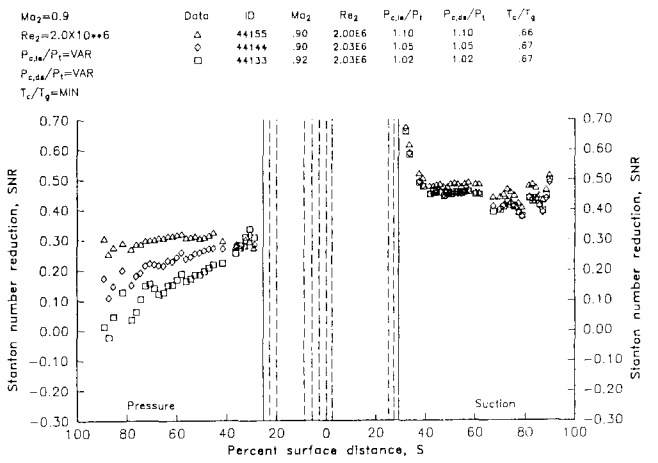

(a)T_c/T_g = MIN

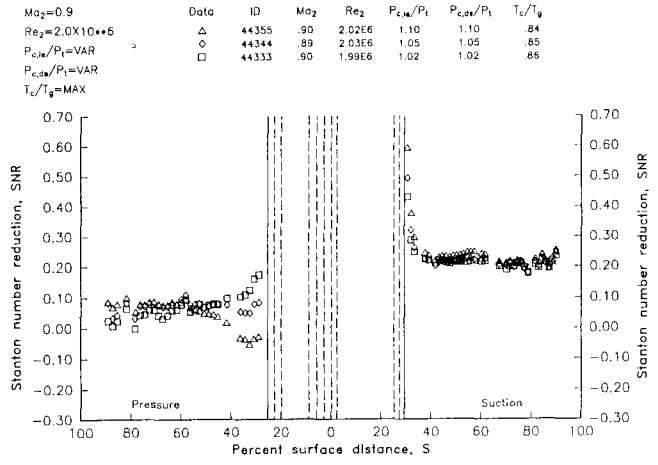

(b)T_c/T_g = MAX

Figure 19. Effects of leading edge and downstream blowing on Stanton number reduction.

CONCLUSIONS

The results from this experiment have provided a data base for characterizing the effects of downstream film cooling with and without leading edge (showerhead) film cooling on external heat transfer of the C3X airfoil.

Static pressure data indicate that vane surface static pressure is independent of downstream and leading edge blowing over the range investigated.

The external heat transfer data indicate that considerable cooling can be attained by downstream film cooling. The downstream film cooling process is shown to be a complex function of mainly two competing mechanisms; (i) the thermal dilution, due to the injection of relatively cold fluid, which decreases heat transfer to the airfoil, and (ii) turbulence augmentation, due to the injection process, which increases heat transfer to the airfoil. It is also observed that favorable cooling effects actually reverse as the coolant-to-gas temperature ratio are varied.

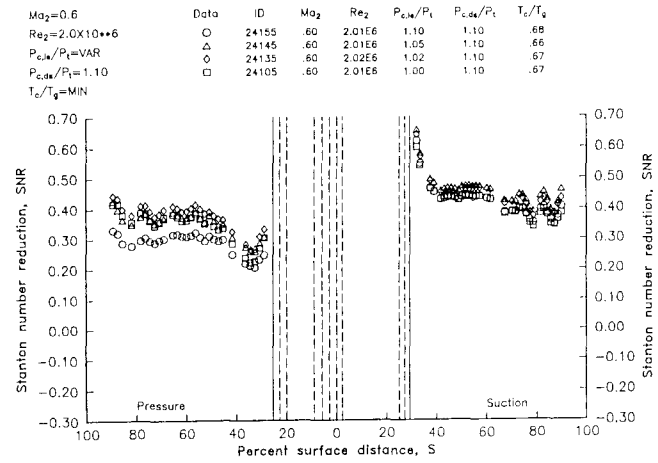

Figure 20. Effects of variable leading edge blowing with constant downstream blowing on Stanton number reduction.

The pressure surface of the airfoil is shown to exhibit a considerably higher degree of sensitivity to the combined effect of turbulence augmentation and thermal dilution. At moderate blowing strengths ($P_c/P_t > 1.0$), the pressure surface shows considerable dependence on blowing strength, while the suction surface is insensitive to variations in blowing strength, due to the coolant flow being choked and causing no significant change in blowing ratio. However at low blowing strengths ($P_c/P_t < 1.00$), the suction surface also shows a dependence on blowing strength. Also, the heat transfer levels are significantly dependent on thermal dilution, to the extent that at high levels of thermal dilution, the adverse turbulence augmentation effect is negligible. The data also indicate that, at high thermal dilution levels (i.e. low coolant-to-gas temperature ratio), the film cooling effects are relatively insensitive to exit Mach numbers; and higher favorable film cooling effects are seen at higher exit Reynolds numbers. Conversely, at low thermal dilution levels (i.e., high coolant-to-gas temperature ratio), film cooling effects are dependent on exit Mach number; and lesser effects due to exit Reynolds number are seen.

ACKNOWLEDGMENTS

The investigation reported herein was performed by Allison Gas Turbine Division with portions of the funding provided by NASA-Lewis Research Center under contract NAS 3-24619. The authors gratefully acknowledge the technical assistance of the NASA program manger, Mr. H. J. Gladden, and his cooperation in allowing the publication of this paper.

In addition, the authors wish to acknowledge the contributions made by Mr. R. M. Kaufman and Dr. B. K. Sultanian towards acquiring and analyzing the results reported herein.

REFERENCES

Camci, G., 1988. "An Experimental and Numerical Investigation of Near Cooling Hole Heat Fluxes on a Film Cooled Turbine Blade,", ASME Paper No. 88-GT-9.

Camci, G. and Arts, T., 1985a. "Experimental Heat Transfer Investigation Around the Film Cooled Leading Edge of a High Pressure Gas Turbine Rotor Blade," ASME Journal of Engineering for Gas Turbines and Power, Vol. 107, pp. 1016-1021.

Camci, C. and Arts, T., 1985b. "Short Duration Measurements and Numerical Solutions of Heat Transfer along the Suction Side of a Film-Cooled Gas Turbine Blade," ASME Paper No. 85-GT-111.

Goldstein, R. J. and Chen, H. P., 1985. "Film Cooling on A Gas Turbine Blade Near the End Wall," Journal of Engineering for Gas Turbines Power, Vol. 107, pp. 117-122.

Horton, F. G., Schultz, D. L., and Forest, A. E., 1985. "Heat Transfer Measurements with Film Cooling on Turbine Blade Profile in Cascade," ASME Paper No. 85-GT-117.

Hylton, L. D., Nirmalan, V., Sultanian, B. K., and Kaufman, R. M., 1987. "Turbine Airfoil Film Cooling," Turbine Engine Hot Section Technology - 1987, NASA CP-2493.

Hylton, L. D., Nirmalan, V., Sultanian, B. K., and Kaufman, R. M., 1988. "The Effects of Leading Edge and Downstream Film Cooling on Turbine Vane Heat Transfer," NASA CR-182133.

Kline, S. J. and McClintock, F. A., 1953. "Describing Uncertainties in Single-Sample Experiments," Mechanical Engineering, January.

Moffat, R. J., 1986. "Turbine Blade Cooling," In Heat Transfer and Fluid Flow in Rotating Machinery, W.-J. Yang, Ed., Hemisphere Publishing Corporation, Washington, D.C., pp. 1-26.

Nealy, D. A., Mihelc, M. S., Hylton, L. D., and Gladden, H. J., 1984. "Measurements of Heat Transfer Distribution over the Surfaces of Highly Loaded Turbine Nozzle Guide Vanes," ASME Journal of Engineering for Gas Turbines and Power, Vol. 106, pp. 149-158.

Turner, A. B., 1971, "Local Heat Transfer Measurements on a Gas Turbine Blade," Journal of Mechanical Engineering Sciences, Vol.13, pp. 1-12.

Turner, E. R., Wilson, M. D., Hylton, L. D., and Kaufman, R. M., 1985, "Turbine Vane External Heat Transfer, Vol. I, Analytical and Experimental Evaluation of Surface Heat Transfer Distributions with Leading Edge Showerhead Film Cooling," NASA CR-174827.